

Electronic structures and optical properties of realistic transition metal dichalcogenide heterostructures from first principles

Hannu-Pekka Komsa¹ and Arkady V. Krasheninnikov^{1,2}

¹*Department of Physics, University of Helsinki, P.O. Box 43, 00014 Helsinki, Finland and*

²*Department of Applied Physics, Aalto University, P.O. Box 11100, 00076 Aalto, Finland*

(Dated: September 12, 2013)

We calculate from first principles the electronic structure and optical properties of a number of transition metal dichalcogenide (TMD) bilayer heterostructures consisting of MoS₂ layers sandwiched with WS₂, MoSe₂, MoTe₂, BN, or graphene sheets. Contrary to previous works, the systems are constructed in such a way that the unstrained lattice constants of the constituent incommensurate monolayers are retained. We find strong interaction between the Γ -point states in all TMD/TMD heterostructures, which can lead to an indirect gap. On the other hand, states near the K-point remain as in the monolayers. When TMDs are paired with BN or graphene layers, the interaction around Γ -point is negligible, and the electronic structure resembles that of two independent monolayers. Calculations of optical properties of the MoS₂/WS₂ system show that even when the valence and conduction band edges are located in different layers, the mixing of optical transitions is minimal, and the optical characteristics of the monolayers are largely retained in these heterostructures. The intensity of interlayer transitions is found to be negligibly small, a discouraging result for engineering the optical gap of TMDs by heterostructuring.

I. INTRODUCTION

Transition metal dichalcogenide (TMD) layered materials^{1,2} possess unique electronic,³ optical,⁴⁻⁶ and mechanical properties.⁷⁻⁹ Moreover, when used together with graphene and BN sheets, they show promise for construction of ultra-thin flexible devices based solely on two-dimensional layers.^{10,11} First steps in this direction have recently been demonstrated with the fabrication of transistors, inverters, and memory cells.¹²⁻¹⁵

In order to further expand the range of properties achievable by the TMD materials, the pristine systems may be modified through doping¹⁶⁻¹⁹ or alloying,²⁰⁻²² and also by modifying the layer stacking. Considering the dramatic change from indirect gap in bilayer MoS₂ to direct gap in monolayer,^{4,23} significant changes might also be expected when layers of different materials are stacked. For instance, recent computational studies suggested that the band gap may be engineered by constructing TMD/TMD heterostructures.²⁴⁻²⁶ However, several questions still remain open.

First, in the case of MoS₂/WS₂, it was shown that the valence band maximum (VBM) and conduction band minimum (CBM) are located in different layers (often referred to as “type-II alignment”). Through a simple picture of single-particle band structure, such band alignment would lead to decreased band gaps. However, this is true only for the fundamental gap measured as a difference between the electron affinity and ionization potential, but does not necessarily hold for the optical transitions. In essence, it is not clear what kind of transition spectrum such systems would show.

Second, theoretical studies of other TMD/TMD heterostructures (such as MoS₂/MoSe₂) suffer from the problem of incommensurate lattice constants, which has so far been circumvented by only considering strongly strained systems. The energy cost for straining both lay-

ers and the lack of barrier for relaxing to unstrained state suggest that formation of strained heterostructures is unlikely. Indeed, during epitaxial growth of TMD monolayers on graphene, the lattice constants were found to be very close to those of isolated monolayers, although with some preferential orientation among the layers.²⁷ As strain is known to give rise to dramatic changes in the electronic properties of 2D systems,^{10,28-30} it is difficult to distinguish which features then originate from the stacking and which are due to the strain artificially introduced into the system due to computational limitations.

In this work, by using first-principles calculations, we study bilayer heterostructures consisting of MoS₂ and WS₂, MoSe₂, MoTe₂, BN, or graphene. By constructing heterostructure models where both constituent layers retain their optimized lattice constant and including the electron-hole interactions through the solution of the Bethe-Salpeter equation (BSE) for the MoS₂/WS₂ system, we go beyond the body of previous work and give answers to the open questions listed above. We also discuss the optical properties of the systems with incommensurate lattices, and demonstrate that the optical characteristics of the monolayers are largely retained in these heterostructures.

II. METHODS

All calculations are carried out with plane waves and the projector-augmented wave scheme as implemented in VASP.^{31,32} The plane wave cutoff is set to 500 eV. Exchange-correlation contributions are treated with Perdew-Burke-Ernzerhof³³ (PBE) functional including empirical dispersion corrections (PBE-D) proposed by Grimme.³⁴ The ions are relaxed until forces are converged to less than 2 meV/Å. In selected cases, we also cross-

check our PBE-D results against ab-initio dispersion corrected functionals, PW86R-VV10 and AM05-VV10sol, which have been shown to give layer distances in excellent agreement with experiment.^{35–37}

Since the constituent monolayers have generally differing lattice constants, special care is needed in the construction of the atomic models in such a way that the strain is minimized. Our approach is illustrated in Fig. 1. Let us denote the primitive cell basis vectors of a 2D material i as $\{a_i, b_i\}$. The supercell basis vector may be constructed as $n_i a_i + m_i b_i$, where n_i and m_i are integers. The second basis vector is always oriented at an 120° angle. We then search for a set of integers such that the magnitude of the supercell basis vectors in materials i and j approximately match: $|n_i a_i + m_i b_i| \approx |n_j a_j + m_j b_j|$. In practice, we choose the smallest supercell for which the strain is less than 1%. The resulting structures contain 75–102 atoms. The two integers defining our models are listed in Table I. For all the heterostructures in this work, one layer is always MoS₂. Therefore, we have fixed the lattice constant of MoS₂ to the optimized value of 3.18 Å, and squeezed or stretched the other layer slightly. These resulting lattice constants (compared to the optimized ones) are also given in Table I together with the relative orientation of the layers as determined by the construction scheme. The perpendicular lattice vector c is 25.44 Å. We employ $4 \times 4 \times 1$ k-point sampling throughout.

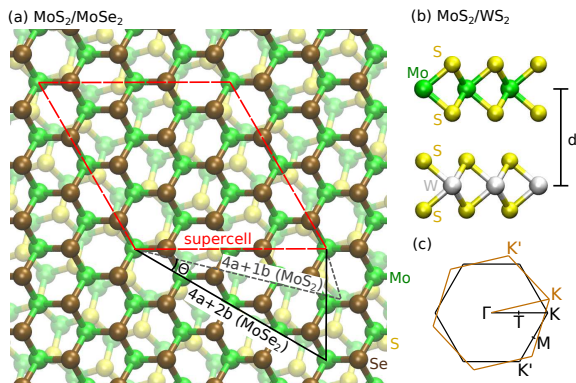


FIG. 1. (Color online) (a) Top view of MoS₂/MoSe₂ bilayer heterostructure as modeled in our supercell approach. The construction of the supercell basis vectors ($n_i a_i + m_i b_i$) is also illustrated. (b) Side view of the MoS₂/WS₂ heterostructure showing the adopted stacking similar to 2H-polytype of MoS₂. The definition for layer distance d is indicated. (c) Schematic demonstration of the overlap of the primitive cell Brillouin zones from the MoS₂/MoSe₂ system.

The calculated, as well as experimental, lattice constants of MoS₂ and WS₂ are very close. Thus, the heterostructure can be constructed simply from the primitive cells of MoS₂ and WS₂ with negligible strain. The stacking adopted here corresponds to that found in 2H-MoS₂ i.e., chalcogen sublattice of one layer overlaps with transition metal sublattice of the other layer. Due to the large spin-orbit splitting of VBM states near K-point,

TABLE I. Description of supercell models for the bilayer heterostructures. The integers describing the supercell basis vectors for both layers are given together with the resulting lattice constant of the second slightly strained layer (optimized lattice constant in parentheses) and the angle between the lattices.

system	basis 1	basis 2	a_2	angle
MoS ₂ /WS ₂	a	a	3.18 (3.18)	60.0
MoS ₂ /MoSe ₂	$4a + 1b$	$4a + 2b$	3.31 (3.32)	16.1
MoS ₂ /MoTe ₂	$4a$	$4a + 1b$	3.53 (3.55)	13.9
MoS ₂ /BN	$4a + 1b$	$5a + 1b$	2.50 (2.51)	3.0
MoS ₂ /G	$4a$	$6a + 3b$	2.45 (2.47)	30.0

spin-orbit coupling is included in these calculations. In this case, $12 \times 12 \times 1$ k-point sampling is used.

The band structures are calculated for all systems at the PBE level. The electronic states from the supercell calculations are projected to the primitive cells of each constituent layer, following Ref. 38. Note, that when the layer orientations do not align, also the Brillouin zone high-symmetry points for the two constituent monolayers reside at different points of the reciprocal space, as illustrated in Fig. 1(c). When drawing the band structures, the Brillouin zone segments (e.g. Γ -K) from the two lattices are overlaid. To be more precise, each supercell state is first projected to one of the monolayers and then to the specific Brillouin zone segment of the respective layer. Although the quasiparticle gap from GW is strongly influenced by the size of vacuum, all the main features of the band structure are correctly described by PBE.³⁹ Therefore, when the effects of interlayer interactions on the electronic structure are considered, the PBE level of theory is deemed sufficient.

Electron-hole interactions need to be accounted for when optical absorption spectra are considered. In the calculations of optical spectra, we rely on the single-shot G_0W_0 procedure together with solution of the Bethe-Salpeter equation in the Tamm-Dancoff approximation.^{40,41} Due to computational cost involved, this is only done for the MoS₂/WS₂ system. Hybrid functionals are known to improve the starting electronic structure,^{42,43} and thus the G_0W_0 is solved on top of HSE band structure. Atomic geometry is obtained using PBE-D with lattice constant $c = 18.67$ Å, which leads to Mo-W distance of $d = 12.49$ Å over the vacuum region. Note that unlike the GW gaps, the optical transitions from BSE are fairly insensitive to the amount of vacuum in the calculation.^{39,44} Spin-orbit interaction is fully accounted for. The adopted $12 \times 12 \times 1$ k-point mesh is mostly sufficient for proper description of excitons.^{30,45} For monolayer, we have 192 states in the calculation and for bilayer 288 states (scaled with the supercell volume). Plane wave cutoffs are 280 eV and 200 eV for the wave functions and for the response functions, respectively. These parameters were carefully optimized to reproduce converged absorption spectrum.

III. MoS₂/WS₂ HETEROSTRUCTURE

A. Electronic structure

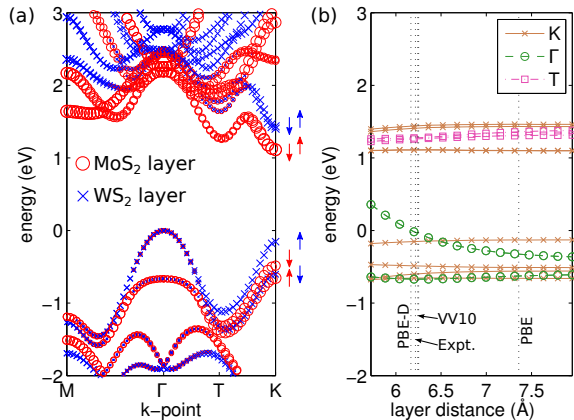


FIG. 2. (Color online) (a) Band structure of MoS₂/WS₂ heterostructure. Projection to MoS₂ layer is denoted by red (circles) and to WS₂ by blue (crosses). The spin orientations of the wave functions at the K/K'-point are also denoted. (b) The energies for the band edge states as a function of the interlayer distance d [cf. Fig. 1(b)]. The vertical dotted lines denote distances calculated with various functionals (the two VV10-type functionals give nearly identical results) and experimental value evaluated from the average of bulk MoS₂ and WS₂.

We first consider the MoS₂/WS₂ heterostructure, for which the geometry and stacking is shown in Fig. 1(b). The band structure in Fig. 2(a) shows the same main features as reported in Refs. 24 and 25. In addition, the localization of the states to the two constituent monolayers are highlighted. Around Γ -point, the VBM states show appreciable weight in both layers. On the other hand, the states around K-point are strictly localized to one of the monolayers: VBM at the K-point is completely localized to WS₂ and CBM to MoS₂. The alignment is similar to that expected from the ionization potentials,^{46,47} indicating that the states also retain their energy position with respect to vacuum level. The mixing around the Γ -point is due to interaction of the constituent monolayer states, which also leads to strong shift (or split) of the energy levels. As a result, the valence band Γ -point states are pushed 0.15 eV higher than the K-point states, thus making the gap indirect.

The sensitivity of the VBM state at the Γ -point to the interlayer interactions may be immediately understood through inspection of the constituent wave functions. The wave functions at the valence and conduction band edges are shown in Fig. 3 for MoS₂. They are very similar for other TMDs. At the K-point, both for the VBM and the CBM, wave functions are localized within the transition metal sublattice. On the contrary, VBM at the Γ -point shows lobes extending out from the sulfur

atoms. These states will interact strongly (if also energetically close), when TMD layers are brought in contact. This is further illustrated in Fig. 2(b), where the band edge positions are plotted as a function of the layer separation d . The Γ -point states are seen to move strongly as the layers are brought in contact, while the states around K- and T-valleys remain largely unaffected. The gap becomes indirect at $d < 6.47$ Å, which is fulfilled for all considered vdW-corrected functionals. The layer distance calculated with the PBE-D, PW86R-VV10, and AM05-VV10sol functionals are $d = 6.17$, $d = 6.25$, and $d = 6.24$ Å, respectively. PBE shows essentially no binding and gives the minimum at $d = 7.36$ Å. Note that the experimental distances in both bulk MoS₂ and in bulk WS₂ are similar and would yield approximately $d = 6.22$ Å, in excellent agreement with the results calculated using the vdW-corrected functionals.

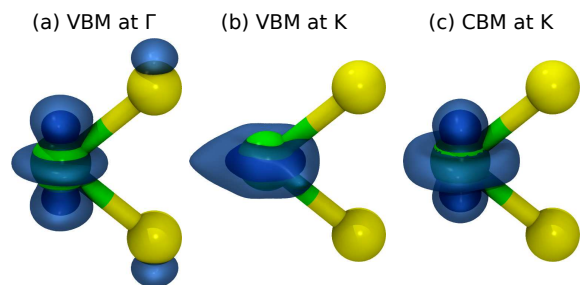


FIG. 3. (Color online) Partial charge density isosurfaces (blue) at 0.37 (transparent) and 1.2 (solid) e/nm³ for selected wave functions of monolayer MoS₂.

B. Optical properties

It was suggested previously, that due to the type-II alignment of band edges in many of these heterostructures, the optical band gap would also decrease and that the excitons would have electron and hole localized to different layers.^{24–26} In order to see if this is indeed the case, we calculated the optical absorption spectrum by solving the Bethe-Salpeter equation. Since the simulation cell for MoS₂/WS₂ heterostructure is small, computationally heavy $GW+BSE$ calculations can be performed. In addition, the orientation of layers is likely to be “correct” in a sense that it corresponds to the minimum energy configuration.

As seen above, the VBM of this system is located at the Γ -point. However, the indirect transitions do not show up in the absorption spectrum, for which the direct transitions at around K-point are known to dominate,^{4,39,48} and we thus concentrate on the latter. Nevertheless, at K-point the VBM is localized in the WS₂ layer and the CBM in the MoS₂ layer. The calculated absorption spectra for MoS₂ and WS₂ monolayers and for the MoS₂/WS₂ heterostructure are shown in Fig. 4. We first note that the calculated energies for the lowest A/B transitions

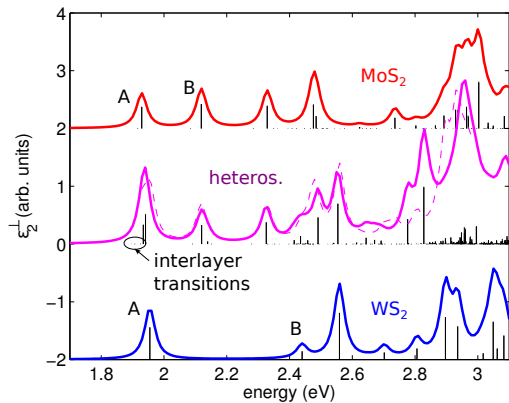


FIG. 4. (Color online) The optical absorption spectrum of MoS₂/WS₂ heterostructure (middle) together with the spectra from monolayer MoS₂ (top) and WS₂ (bottom). The vertical lines denote the actual calculated transition energies and intensities. Absorption spectra are evaluated through application of 0.02 eV Lorentzian broadening. Overlaid with the explicitly calculated heterostructure spectrum, the sum of the monolayer spectra is also plotted (dashed line). Interlayer transitions are present, but have negligible intensities.

in the monolayer systems (1.93/2.12 eV for MoS₂ and 1.96/2.44 eV for WS₂) are in good agreement with the experimental ones (1.9/2.1 eV for MoS₂⁴⁹ and 2.0/2.4 eV for WS₂^{48,50}). The optical response from MoS₂ and WS₂ monolayers are of roughly equal intensity. Turning now to the optical spectrum of the heterostructure, it appears to hold all the same features as in the monolayers and at the same energies. In fact, the total spectrum can be well approximated by simply summing up the monolayer spectra as shown by dashed line in Fig. 4. In order to analyze the character of each transition S , we have inspected in more detail the electron-hole amplitude matrix A_{vck}^S ,⁴¹ where v , c , and \mathbf{k} index valence band states, conduction band states, and \mathbf{k} -points, respectively. This analysis shows that all optically active transitions are comprised of direct intralayer transitions. Note that with the adopted stacking, K-point of MoS₂ coincides with K' point of WS₂ and thus the spin orientations of the MoS₂ and WS₂ VBM states are opposite, as shown in Fig. 2(a). Interlayer transitions were also found, but their intensities are close to zero, and thus do not contribute to the absorption spectrum in Fig. 4. These transitions reach only about 50 meV below the A peak, which is clearly less than that expected from the band alignment. Due to spatial separation, the binding energy becomes smaller, but relaxation of optically active intralayer exciton to optically inactive interlayer exciton is possible.

Thus, engineering of the optical band gap by stacking up suitably aligned monolayers, as previously suggested, does not appear to work. On the other hand, it allows one to achieve stronger monolayer-like optical absorption

from the layered TMD materials by simply stacking them together. While our calculations do not give the dynamics of various scattering and recombination mechanisms, it is surely possible that the photoluminescence spectrum could be modified by the interlayer excitons. Relaxation to interlayer excitons could be particularly useful in separating and collecting optically excited electron-hole pairs, and at the same time eliminating the direct recombination channel, in photodetector or solar cell applications.

IV. MoS₂ WITH MoSe₂, MoTe₂, BN, AND GRAPHENE

A. Electronic structure

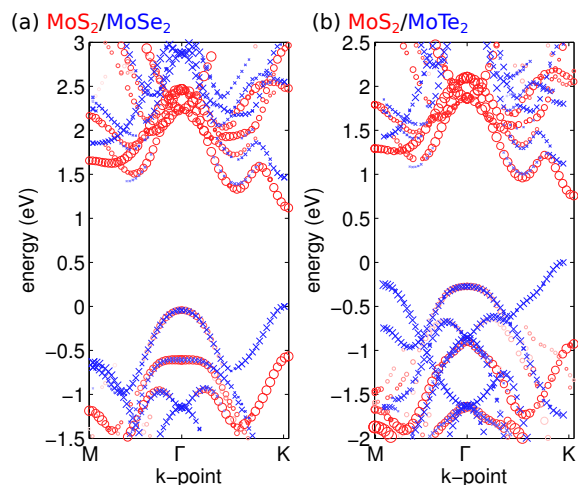


FIG. 5. (Color online) Band structures of (a) MoS₂/MoSe₂ and (b) MoS₂/MoTe₂ heterostructures. Circles (red) denote projections to MoS₂ layer (opacity) and to the corresponding reciprocal space directions (size of the marker). Crosses (blue) denote similarly projections to MoSe₂ (a) and MoTe₂ (b) layers.

We next study electronic structure of the incommensurate systems. The band structures of MoS₂/MoSe₂ and MoS₂/MoTe₂ are shown in Fig. 5(a,b). The states from the supercell calculation are projected to the corresponding primitive cells of each layer. Similar to the MoS₂/WS₂ system, the K-point states retain their monolayer character, but the Γ -point states are split with a small mixing of the wave function character. Band structure of MoS₂/MoTe₂ looks somewhat different, as the MoS₂ VBM couples to the second highest VBM state of MoTe₂. In both cases, the gap is direct in a sense that both the VBM and CBM are located at the K-point, although again these states are localized in different monolayers in a type-II alignment. We note, that the layer distance calculated with the PBE-D and PW86R-VV10 functionals again agree, both yielding 6.65 Å.

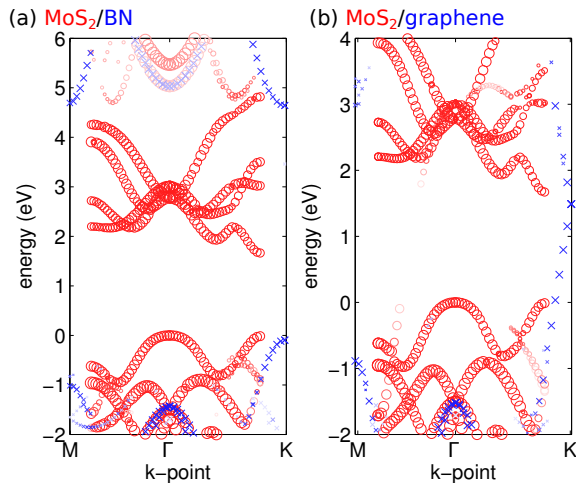


FIG. 6. (Color online) Band structures of (a) MoS_2/BN and (b) $\text{MoS}_2/\text{graphene}$ heterostructures. Notation as in Fig. 5. For each layer, the band structure is plotted up to its first Brillouin zone boundary. Due to different lattice constants, this boundary is located at different wavevectors.

The band structure of MoS_2/BN is shown in Fig. 6(a). In this heterostructure, there are small corrugations in the BN layer: the layer distance is largest for B atoms on top of Mo, and smallest for B atoms on top of the center-of-hexagon of MoS_2 . However, the effect is small and does not affect the band structure. The BN layer has practically no effect on the Γ -point band edge of MoS_2 . The Γ - and K-point edges are energetically close and similar to that found for monolayer MoS_2 . In these calculations the K-point was below the Γ -point by 15 meV, but inclusion of spin-orbit coupling is expected to push VBM at K-point above the Γ -point valley. The VBM of BN is close to, but below of, the VBM of MoS_2 , thereby yielding a type-I alignment.

The band structure of $\text{MoS}_2/\text{graphene}$ is shown in Fig. 6(b). Similar to BN, the interaction with MoS_2 states around the Γ -point, as well as around K-point, is negligible. The Dirac-point of graphene is slightly below CBM of MoS_2 in agreement with previous study.⁵¹

In order to understand the effects of interlayer interactions more generally, the band edge positions from all considered semiconducting heterostructure systems are collected in Fig. 7 together with the corresponding edges from the respective monolayer systems. Several trends can be observed: (i) For TMD/TMD heterostructures, the nature of the VBM wave functions around Γ -point leads to strongly split states. The magnitude of the splitting depends on the position of the states prior to the construction of the heterostructure. This behavior is akin to that found in bilayer TMD systems or even in simple diatomic molecules. We cannot directly probe the sensitivity of splitting on orientation, but as it is observed in all systems here, we expect the orientation to have small effect on the splitting. (ii) Both the VBM and

CBM states around K-point are consistently very close to those of the respective monolayers. As discussed above, this is due to the wave functions being confined in the transition metal sublattice. The small shifts of 0.1–0.2 eV are caused by formation of interface dipole between the layers. (iii) BN and graphene work well to “insulate” the TMD monolayer so that their electronic structures remains very similar to the isolated layers, also around the Γ -point.

The TMD/TMD heterostructures examined so far all yielded type-II alignment, which may be advantageous in separating electron/hole pairs. On the other hand, in order to maximize photoemission, VBM and CBM should both reside at K-point and localized to the same monolayer (i.e., type-I alignment). Among the structures studied so far, MoS_2/BN was the only one fulfilling these conditions. This should also hold for other TMD/BN heterostructures. In addition, using the above trends and the position of band edges in isolated monolayers^{46,47}, the following systems are also expected to show type-I alignment: $\text{MoTe}_2/\text{WSe}_2$, $\text{MoSe}_2/\text{WS}_2$, $\text{HfS}_2/\text{ZrSe}_2$.

Naturally, the monolayer-monolayer interactions discussed within this work are also applicable when substrate-monolayer interactions are considered. For instance, MoS_2 on BN substrate should still retain electronic structure very similar to that of a monolayer MoS_2 . In fact, such system was found to work very well for optical studies in Ref. 49. In case of TMD substrates, or more generally whenever there is strong interaction at Γ -point with the substrate, MoS_2 will easily become indirect gap due to the close energies of the valence band maxima at Γ - and K-points, whereas WS_2 , MoSe_2 , or MoTe_2 are expected to retain their direct gaps.

B. Optical properties

The position of the band edges discussed above is naturally of importance for the optical properties as far as the valley population is concerned. The incommensurate nature of the heterostructures considered here also introduces a new issue of mismatch in valley location in the reciprocal space. That is, the wave vector corresponding to the K-point of the two monolayers have different length and orientation. For many of the TMD/TMD structures, the lengths are reasonably close, but the orientation of the layers is unknown. If the heterostructure is constructed by manually placing monolayers on top of each other,⁵² the orientation is likely to be dominated by the deposition process and the layers do not reorient after that. If the heterostructure is constructed during growth or restacking of layers exfoliated in liquid,⁵³ the orientation might be determined by the total energy of stacking.

Since the K-points are aligned in MoS_2/WS_2 , this system is expected to show the strongest mixing in the optical transitions and the mixing should become smaller in TMD/TMD systems where K-points are misaligned.

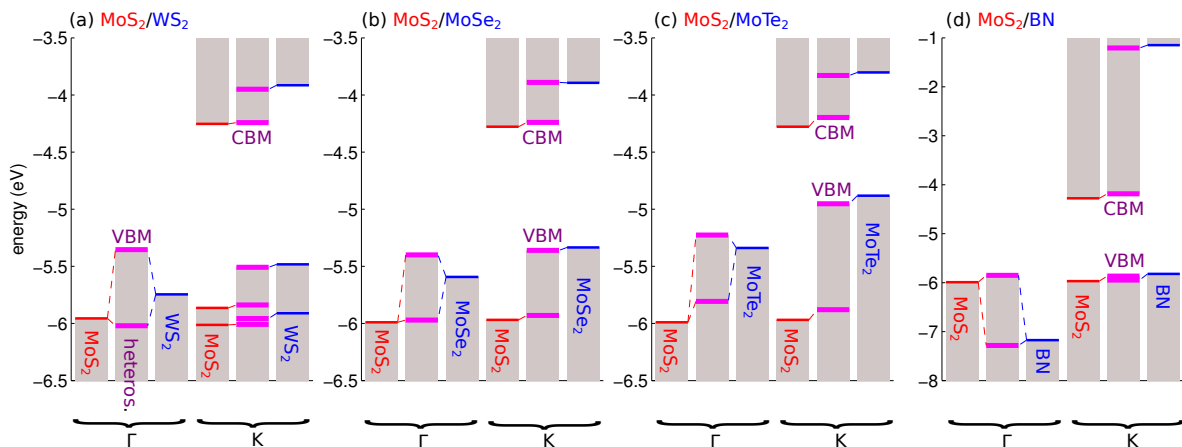


FIG. 7. (Color online) Diagrams illustrating the interaction of band edge states around Γ - and K -points as the heterostructure is constructed from the respective monolayers. The energies are given with respect to the vacuum level.

In the cases of TMD/BN and TMD/graphene, there is very little mixing of the states around the band edges. Since the transitions were seen to be largely decoupled in the MoS_2/WS_2 system, it therefore seems well justified to conclude that for all heterostructures examined in this work the optical absorption spectrum should be well approximated by the sum of its monolayer constituents.

When interlayer excitons are considered, the misalignment of K -points would lead to indirect interlayer excitons. Although physically interesting, carrying out full $GW+BSE$ calculations on these systems is computationally demanding, and thus beyond the scope of this paper.

V. CONCLUSIONS

A set of transition metal dichalcogenide heterostructures were studied via first-principles calculations. The adopted computational scheme enables us to study unstrained systems, thereby moving beyond the artificially strained or naturally commensurate systems considered previously. With regards to the electronic structure, we find that the VBM at Γ -point is very sensitive to interlayer interaction in TMD/TMD heterostructures. Con-

sequently this determines whether VBM is located at the Γ or K -point. On the other hand, heterostructures with graphene or BN show only negligible interaction. Furthermore, we calculated and analyzed the optical transitions in the MoS_2/WS_2 system. The optical properties were found to be only very weakly affected by the interlayer interactions. Novel optical characteristics of monolayer TMDs should be largely retained even when stacked with other layered materials, which should prove useful for amplifying their optical response. However, engineering the optical gap through heterostructuring does not appear to work. Optically inactive interlayer excitons were also found that are of interest in light harvesting applications. We hope our results will guide and motivate future experiments in constructing layered structures and studying their unique optoelectronic properties.

ACKNOWLEDGMENTS

We acknowledge financial support by the Academy of Finland through projects 218545 and 263416, the University of Helsinki Funds. We also thank CSC Finland for generous grants of computer time.

¹ J. Wilson and A. Yoffe, *Adv. Phys.* **18**, 193 (1969).

² R. Tenne, L. Margulis, M. Genut, and G. Hodes, *Nature* **360**, 444 (1992).

³ B. Radisavljevic, A. Radenovic, J. Brivio, V. Giacometti, and A. Kis, *Nat. Nanot.* **6**, 147 (2011).

⁴ K. F. Mak, C. Lee, J. Hone, J. Shan, and T. F. Heinz, *Phys. Rev. Lett.* **105**, 136805 (2010).

⁵ D. Xiao, G.-B. Liu, W. Feng, X. Xu, and W. Yao, *Phys. Rev. Lett.* **108**, 196802 (2012).

⁶ K. F. Mak, K. He, C. Lee, G. H. Lee, J. Hone, T. F. Heinz, and J. Shan, *Nat. Mater.* **12**, 207 (2013).

⁷ I. Kaplan-Ashiri, S. R. Cohen, K. Gartsman, V. Ivanovskaya, T. Heine, G. Seifert, I. Wiesel, H. D. Wagner, and R. Tenne, *Proc. Natl. Acad. Sci. U.S.A.* **103**, 523 (2006).

⁸ S. Bertolazzi, J. Brivio, and A. Kis, *ACS Nano* **5**, 9703 (2011).

⁹ J. Pu, Y. Yomogida, K.-K. Liu, L.-J. Li, Y. Iwasa, and T. Takenobu, *Nano Lett.* **12**, 4013 (2012).

¹⁰ K. S. Novoselov and A. H. Castro Neto, *Physica Scripta* **T146**, 014006 (2012).

- ¹¹ Q. H. Wang, K. Kalantar-Zadeh, A. Kis, J. N. Coleman, and M. S. Strano, *Nat. Nanot.* **7**, 699 (2012).
- ¹² L. Britnell, R. V. Gorbachev, R. Jalil, B. D. Belle, F. Schedin, A. Mishchenko, T. Georgiou, M. I. Katsnelson, L. Eaves, S. V. Morozov, N. M. R. Peres, J. Leist, A. K. Geim, K. S. Novoselov, and L. A. Ponomarenko, *Science* **335**, 947 (2012).
- ¹³ W. J. Yu, Z. Li, H. Zhou, Y. Chen, Y. Wang, Y. Huang, and X. Duan, *Nat. Mater.* **12**, 246 (2013).
- ¹⁴ S. Bertolazzi, D. Krasnozhan, and A. Kis, *ACS Nano* **7**, 3246 (2013).
- ¹⁵ T. Georgiou, R. Jalil, B. D. Belle, L. Britnell, R. V. Gorbachev, S. V. Morozov, Y.-J. Kim, A. Gholinia, S. J. Haigh, O. Makarovskiy, L. Eaves, L. A. Ponomarenko, A. K. Geim, K. S. Novoselov, and A. Mishchenko, *Nat. Nanot.* **8**, 100 (2013).
- ¹⁶ H.-P. Komsa, J. Kotakoski, S. Kurasch, O. Lehtinen, U. Kaiser, and A. V. Krasheninnikov, *Phys. Rev. Lett.* **109**, 035503 (2012).
- ¹⁷ H.-P. Komsa, S. Kurasch, O. Lehtinen, U. Kaiser, and A. V. Krasheninnikov, *Phys. Rev. B* **88**, 035301 (2013).
- ¹⁸ L. Yadgarov, R. Rosentsveig, G. Leituss, A. Albu-Yaron, A. Moshkovich, V. Perfilov, R. Vasic, A. I. Frenkel, A. N. Enyashin, G. Seifert, L. Rapoport, and R. Tenne, *Angew. Chem. Int. Ed.* **51**, 1148 (2012).
- ¹⁹ Y. C. Cheng, Z. Y. Zhu, W. B. Mi, Z. B. Guo, and U. Schwingenschlöggl, *Phys. Rev. B* **87**, 100401 (2013).
- ²⁰ H.-P. Komsa and A. V. Krasheninnikov, *J. Phys. Chem. Lett.* **3**, 3652 (2012).
- ²¹ J. Kang, S. Tongay, J. Li, and J. Wu, *J. Appl. Phys.* **113**, 143703 (2013).
- ²² D. O. Dumcenco, H. Kobayashi, Z. Liu, Y.-S. Huang, and K. Suenaga, *Nat. Comm.* **4**, 1351 (2013).
- ²³ A. Kuc, N. Zibouche, and T. Heine, *Phys. Rev. B* **83**, 245213 (2011).
- ²⁴ K. Kośmider and J. Fernández-Rossier, *Phys. Rev. B* **87**, 075451 (2013).
- ²⁵ H. Terrones, F. López-Urías, and M. Terrones, *Scientific Reports* **3**, 1549 (2013).
- ²⁶ L. Kou, T. Frauenheim, and C. Chen, *The Journal of Physical Chemistry Letters* **4**, 1730 (2013).
- ²⁷ Y. Shi, W. Zhou, A.-Y. Lu, W. Fang, Y.-H. Lee, A. L. Hsu, S. M. Kim, K. K. Kim, H. Y. Yang, L.-J. Li, J.-C. Idrobo, and J. Kong, *Nano Lett.* **12**, 2784 (2012).
- ²⁸ W. S. Yun, S. W. Han, S. C. Hong, I. G. Kim, and J. D. Lee, *Phys. Rev. B* **85**, 033305 (2012).
- ²⁹ P. Johari and V. B. Shenoy, *ACS Nano* **6**, 5449 (2012).
- ³⁰ H. Shi, H. Pan, Y.-W. Zhang, and B. I. Yakobson, *Phys. Rev. B* **87**, 155304 (2013).
- ³¹ G. Kresse and J. Hafner, *Phys. Rev. B* **47**, 558 (1993).
- ³² G. Kresse and J. Furthmüller, *Comput. Mat. Sci.* **6**, 15 (1996).
- ³³ J. P. Perdew, K. Burke, and M. Ernzerhof, *Phys. Rev. Lett.* **77**, 3865 (1996).
- ³⁴ S. Grimme, *J. Comput. Chem.* **27**, 1787 (2006).
- ³⁵ O. A. Vydrov and T. Van Voorhis, *J. Chem. Phys.* **133**, 244103 (2010).
- ³⁶ T. Björkman, *Phys. Rev. B* **86**, 165109 (2012).
- ³⁷ T. Björkman, A. Gulans, A. V. Krasheninnikov, and R. M. Nieminen, *Phys. Rev. Lett.* **108**, 235502 (2012).
- ³⁸ V. Popescu and A. Zunger, *Phys. Rev. Lett.* **104**, 236403 (2010).
- ³⁹ H.-P. Komsa and A. V. Krasheninnikov, *Phys. Rev. B* **86**, 241201 (2012).
- ⁴⁰ M. Shishkin and G. Kresse, *Phys. Rev. B* **74**, 035101 (2006).
- ⁴¹ M. Rohlfing and S. G. Louie, *Phys. Rev. Lett.* **81**, 2312 (1998).
- ⁴² P. Rinke, A. Qteish, J. Neugebauer, C. Freysoldt, and M. Scheffler, *New J. Phys.* **7**, 126 (2005).
- ⁴³ F. Bechstedt, F. Fuchs, and G. Kresse, *phys. stat. sol. (b)* **246**, 1877 (2009).
- ⁴⁴ L. Wirtz, A. Marini, and A. Rubio, *Phys. Rev. Lett.* **96**, 126104 (2006).
- ⁴⁵ A. Molina-Sánchez, D. Sangalli, K. Hummer, A. Marini, and L. Wirtz, *Phys. Rev. B* **88**, 045412 (2013).
- ⁴⁶ H. Jiang, *J. Phys. Chem. C* **116**, 7664 (2012).
- ⁴⁷ J. Kang, S. Tongay, J. Zhou, J. Li, and J. Wu, *Appl. Phys. Lett.* **102**, 012111 (2013).
- ⁴⁸ W. Zhao, Z. Ghorannevis, L. Chu, M. Toh, C. Kloc, P.-H. Tan, and G. Eda, *ACS Nano* **7**, 791 (2013).
- ⁴⁹ K. F. Mak, K. He, J. Shan, and T. F. Heinz, *Nat. Nanot.* **7**, 494 (2012).
- ⁵⁰ H. R. Gutiérrez, N. Perea-López, A. L. Elías, A. Berkdemir, B. Wang, R. Lv, F. López-Urías, V. H. Crespi, H. Terrones, and M. Terrones, *Nano Letters* **0**, 0 (2013).
- ⁵¹ Y. Ma, Y. Dai, M. Guo, C. Niu, and B. Huang, *Nanoscale* **3**, 3883 (2011).
- ⁵² Y.-H. Lee, L. Yu, H. Wang, W. Fang, X. Ling, Y. Shi, C.-T. Lin, J.-K. Huang, M.-T. Chang, C.-S. Chang, M. Dresselhaus, T. Palacios, L.-J. Li, and J. Kong, *Nano Lett.* **13**, 1852 (2013).
- ⁵³ J. N. Coleman, M. Lotya, A. O'Neill, S. D. Bergin, P. J. King, U. Khan, K. Young, A. Gaucher, S. De, R. J. Smith, I. V. Shvets, S. K. Arora, G. Stanton, H.-Y. Kim, K. Lee, G. T. Kim, G. S. Duesberg, T. Hallam, J. J. Boland, J. J. Wang, J. F. Donegan, J. C. Grunlan, G. Moriarty, A. Shmeliov, R. J. Nicholls, J. M. Perkins, E. M. Grievson, K. Theuwissen, D. W. McComb, P. D. Nellist, and V. Nicolosi, *Science* **331**, 568 (2011).